Int. J. Therm. Sci. (2001) 40, 30–41

S1290-0729(00)01185-6/FLA

Double diffusive convection in a vertical enclosure filled with anisotropic porous media

Rachid Bennacer [a]*, Abdelwahab Tobbal [a], Hassen Beji [a], Patrick Vasseur [b]

[a] *Université de Cergy-Pontoise, 95031 Neuville-sur-Oise, France*

[b] *École Polytechnique, C.P. 6079, succ "Centre Ville", Montréal, Québec H3C 3A7, Canada*

(Received 26 October 1999, accepted 31 January 2000)

Abstract — This paper summarises a numerical study of double-diffusive natural convection in a rectangular cavity filled with a saturated anisotropic porous medium. The side walls of the cavity are maintained at constant temperatures and concentrations, while the horizontal walls are adiabatic and impermeable. The buoyancy forces that induce the fluid motion are assumed to be cooperative. Numerical results are presented for $10^2 \leq R_T \leq 10^4$, $0 \leq N \leq 30$, $10^{-5} \leq K \leq 10^3$, $1 \leq Le \leq 10$, and $A = 1$, where R_T, N, K, Le and A denote the thermal Rayleigh number, buoyancy ratio, permeability ratio, Lewis number and the aspect ratio. In the two extreme cases of heat-driven ($N \ll 1$) and solute-driven ($N \gg 1$) natural convection, scale analysis is applied to predict the order of magnitudes involved in the boundary layer regime. Also, based on the numerical results, correlations for the average Nusselt and Sherwood numbers are proposed for the range of parameters considered in this study. It is demonstrated that the anisotropic properties of the porous medium considerably modify the heat and mass transfer rates from that expected under isotropic conditions. The Brinkman's extension of Darcy's law is also used in this study to investigate double-diffusive convection in anisotropic porous media with high porosity. © 2001 Éditions scientifiques et médicales Elsevier SAS

double diffusion / thermosolutal / natural convection / porous media / anisotropic

Nomenclature

A aspect ratio of the cavity $= H/L$
D mass diffusivity
Da Darcy number $= K_z/H^2$
g gravitational acceleration
H height of the cavity
K_x permeability along x axis
K_z permeability along z axis
K permeability ratio $= K_x/K_z$
$\overline{K}$ modified permeability ratio $= 1 + K_{cr}/K$
K_{cr} critical permeability ratio
L thickness of the cavity
Le Lewis number $= \alpha/D$
N buoyancy ratio $= \beta_S \Delta S'/(\beta_T \Delta T')$
$\overline{Nu}$ average Nusselt number, equation (10)
p pressure
R_T thermal Rayleigh number $= K_z g \beta_T \Delta T' H/(\alpha \nu)$
R_S solutal Rayleigh number $= R_T NLe$
Ra_T thermal Rayleigh number for a fluid $= R_T/Da$
S dimensionless solute concentration $= (S' - S'_m)/\Delta S'$
S'_m reference solute concentration at the geometric centre of the cavity
$\overline{Sh}$ average Sherwood number, equation (11)
$\Delta S'$ characteristic solute concentration difference $= S'_1 - S'_2$
T dimensionless temperature $= (T' - T'_m)/\Delta T'$
$\Delta T'$ characteristic temperature difference $= T'_1 - T'_2$
u, w dimensionless velocities in x- and z-directions $= (u', w')H/\alpha$
x, z dimensionless Cartesian coordinates $= (x', z')/H$

Greek symbols

α effective thermal diffusivity
β_T coefficient of thermal expansion
β_S coefficient of solutal expansion
δ_T dimensionless thickness of the thermal boundary layer

* Correspondence and reprints.
E-mail address: Rachid.Bennacer@iupgc.u-cergy.fr (R. Bennacer).

δ_S dimensionless thickness of the solute boundary layer
μ dynamic viscosity of the fluid
μ_{eff} apparent dynamic viscosity for Brinkman's model
λ relative viscosity $= \mu_{eff}/\mu$
ν kinematic viscosity of the fluid
ρ density of the fluid

Superscript

$'$ dimensional quantities

Subscript

m reference state

1. INTRODUCTION

Natural convection through anisotropic porous media is of considerable interest in many applications such as in geophysics, hydrology, oil extraction and in various industrial processes, to name but a few. Anisotropy is generally a consequence of a preferential orientation and/or asymmetric geometry of the grains or fibres. Natural convection in such anisotropic porous media has received relatively little attention despite its broad range of applications.

Earlier studies on natural convection in saturated anisotropic porous media have generally been confined to the effects of anisotropy on the development of the convective flow and heat transfer in a porous layer of infinite horizontal extent heated from below. A literature review may be found in the article of Nilsen and Storesletten [1] as well as in the book by Nield and Bejan [2] and Ingham and Pop [3]. Several studies have also been reported concerning natural convection in vertical anisotropic porous layers heated from the side. For instance, the case of a square cavity filled with porous media that are both thermally and hydrodynanically anisotropic has been investigated analytically by Kimura et al. [4] and numerically by Ni and Beckermann [5]. In these studies it was assumed that the principal direction of the permeability and thermal conductivities coincide with the horizontal and vertical coordinate axes. It was demonstrated that the effect of anisotropy on the flow patterns and the overall Nusselt number was significant.

A few studies have also been concerned with anisotropic media where principal axes are non-coincident with the gravity vector. Thus, the onset of convection in an infinite horizontal layer heated from below and cooled from above was investigated by Tyvand and Storesletten [6], Zhang et al. [7] and Mamou et al. [8] for various thermal boundary conditions. The critical Rayleigh number and wave number at marginal stability were predicted in terms of the permeability ratio, the orientation angle of the principal axes and the porous layer aspect ratio. Convection heat transfer in a vertical cavity heated from the side with various thermal boundary conditions have been investigated by Zhang [9], Degan et al. [10] and Degan and Vasseur [11, 12]. All these studies indicate that both the permeability ratio and inclination angle of the principal axes have a strong influence on the flow structure and the heat transfer rate. Numerical results concerning natural convection within horizontal cylinders and concentric cylinders heated isothermally are also discussed in the book by Ingham and Pop [3].

In all the above studies convection is induced by buoyancy forces due to the variations of temperature solely. Recently, interest for flows resulting from the combined action of both temperature and concentration has surged in view of its importance in various engineering problems. Despite this fact relatively little research work has been reported concerning double-diffusive convection in a porous medium, especially when this latter is anisotropic which is the case more often than not. The onset of thermohaline convection in a horizontal anisotropic porous layer has been investigated by Tyvand [13]. The effect of simultaneous vertical anisotropy in permeability, thermal diffusivity and solutal diffusivity was investigated by this author. Nguyen et al. [14] treated the problem of double-diffusive convection in an enclosure filled with two layers of anisotropic porous media. Recently, a numerical study was conducted by Bera et al. [15] on thermosolutal convection within a rectangular enclosure. It was found that anisotropy causes significant changes in the Nusselt and Sherwood numbers.

The present paper describes the natural convection and heat and mass transfer characteristics through a saturated porous rectangular cavity, when the porous matrix has an anisotropic property in permeability. The complete system of governing equations is solved numerically and results are obtained for a large range of the governing parameters. In the two extreme cases of heat-driven and solute-driven natural convection correlations, valid in the boundary layer regime, are proposed to predict the average Nusselt and Sherwood numbers. The results presented here are relevant to proper understanding of double-diffusive natural convection characteristics in anisotropic porous media.

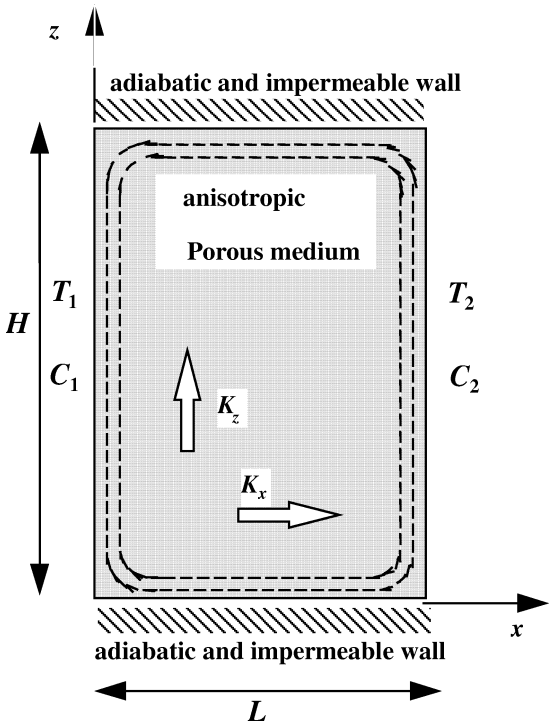

Figure 1. Schematic of the physical model and coordinate system.

2. MATHEMATICAL FORMULATION

The system considered in this study is the rectangular porous cavity shown in *figure 1*. The enclosure is of height H and width L. The porous medium is anisotropic, the principal directions of the permeabilities (K_x and K_z) being assumed to coincide with the horizontal and vertical coordinate axes. The anisotropy in flow permeabilities of the porous medium is then characterised by the permeability ratio $K = K_x/K_z$. The two vertical walls are maintained at uniform and different temperatures and concentrations T_1' and T_2' (S_1' and S_2') while the two horizontal walls are assumed adiabatic and impermeable. The solution that saturates the porous matrix is modelled as a Boussinesq incompressible fluid whose density variation can be expressed as

$$\rho = \rho_{\mathrm{m}}\left[1 - \beta_{\mathrm{T}}\left(T' - T_{\mathrm{m}}'\right) - \beta_{\mathrm{S}}\left(S' - S_{\mathrm{m}}'\right)\right] \qquad (1)$$

where β_{T} and β_{S} are the thermal and concentration expansion coefficients. Subscript m stands for a reference state.

It is assumed that the flow is laminar and that the cavity is long enough in the third (transverse) direction to allow the system to be treated as a two-dimensional rectangular cavity. Also, Soret and Dufour effects on heat and mass diffusion are neglected. The following nondimensional variables are introduced:

$$\begin{aligned}
&(x, y) = \frac{(x', y')}{H}, && p = \frac{p' K_z}{\mu\alpha} \\
&(u, w) = \frac{(u', w')H}{\alpha}, && T = \frac{T' - T_{\mathrm{m}}'}{\Delta T'} \\
&T_{\mathrm{m}} = \frac{T_1' + T_2'}{2}, && \Delta T' = T_1' - T_2' \\
&S = \frac{S' - S_{\mathrm{m}}'}{\Delta S'}, && S_{\mathrm{m}} = \frac{S_1' + S_2'}{2} \\
&\Delta S' = S_1' - S_2'
\end{aligned} \qquad (2)$$

The equations governing the conservation of mass, momentum (generalised Darcy's law), energy and constituent in the solution-saturated porous medium are, in dimensionless form, respectively

$$\frac{\partial u}{\partial x} + \frac{\partial w}{\partial z} = 0 \qquad (3)$$

$$u = -K\,\frac{\partial p}{\partial x} \qquad (4)$$

$$w = -\frac{\partial p}{\partial z} + R_{\mathrm{T}}(T + NS) \qquad (5)$$

$$u\,\frac{\partial T}{\partial x} + w\,\frac{\partial T}{\partial z} = \nabla^2 T \qquad (6)$$

$$u\,\frac{\partial S}{\partial x} + w\,\frac{\partial S}{\partial z} = \frac{1}{Le}\,\nabla^2 S \qquad (7)$$

The nondimensional boundary conditions over the walls of the enclosure are:

$$\begin{aligned}
&x = 0, && u = 0, && T = 0.5, && S = 0.5 \\
&x = \frac{1}{A}, && u = 0, && T = -0.5, && S = -0.5 \\
&z = 0 \text{ or } 1, && w = 0, && \frac{\partial T}{\partial z} = 0, && \frac{\partial S}{\partial z} = 0
\end{aligned} \qquad (8)$$

From the dimensionless equations (3)–(8) it is seen that the present problem is governed by five dimensionless parameters, namely, the thermal Rayleigh number R_{T}, the buoyancy ratio N, the Lewis number Le, the aspect ratio A and the permeability ratio K, defined as

$$\begin{aligned}
&R_{\mathrm{T}} = \frac{K_z g \beta_{\mathrm{T}} \Delta T' H}{\alpha\nu}, && N = \frac{\beta_{\mathrm{S}} \Delta S'}{\beta_{\mathrm{T}} \Delta T'} \\
&Le = \frac{\alpha}{D}, && K = \frac{K_x}{K_z} \\
&A = \frac{H}{L}
\end{aligned} \qquad (9)$$

where g, ν and D are the gravitational acceleration, kinematic viscosity of the fluid and the solute diffusivity, respectively. $\alpha = k/(\rho C_f)$ is the effective thermal diffusivity in porous medium where k is the thermal conductivity of the saturated porous medium and ρC_f the heat capacity of the fluid.

The rate of heat and solute along the vertical walls is determined from the temperature and concentration fields, respectively. The average $\overline{Nu}$ and $\overline{Sh}$ are defined as follows:

$$\overline{Nu} = -\int_0^1 \left.\frac{\partial T}{\partial x}\right|_{x=0} \mathrm{d}z \tag{10}$$

$$\overline{Sh} = -\int_0^1 \left.\frac{\partial S}{\partial x}\right|_{x=0} \mathrm{d}z \tag{11}$$

3. SCALE ANALYSIS

The governing equations (3)–(9) indicate that, in the general case, the quantities of interest involved in the present problem are related to each other in a so complicated way that it is impossible to evaluate their orders of magnitudes by scale analysis. However, when the buoyancy-induced fluid circulation within the enclosure is strong enough, the flow has a boundary layer structure consisting of a core region and two vertical boundary layers. For this situation, for the two limiting cases of heat-driven and solute-driven boundary layer type natural convection, orders of magnitude estimates can be predicted on scaling grounds as done in isotropic problems by Bejan and Khair [16].

3.1. Heat-driven flows

In this section it is assumed that the buoyancy forces that drive the flow are mainly due to the gradients of temperature ($N \ll 1$). In the boundary layer regime, most of the fluid motion is restricted to a thin layer of thickness δ'_T and height H ($\delta'_T \ll H$). In this region the continuity equation (3) requires the following balance:

$$\frac{u}{\delta_T} \sim w \tag{12}$$

where $\delta_T = \delta'_T/H$ is the dimensionless thickness of the vertical boundary layer.

Turning our attention to the momentum balance in the same layer, the following scales are dictated from equations (4) and (5), respectively:

$$u \sim K\,\frac{\Delta p_x}{\delta_T} \tag{13}$$

and

$$(w, \Delta p_z) \sim R_T \tag{14}$$

where Δp_x is the pressure change across the thermal layer and Δp_z the pressure difference between the horizontal boundaries.

The energy equation (6), expressing a balance between convection and conduction of heat, gives

$$\left(\frac{u}{\delta_T}, \omega\right) \sim \left(\frac{1}{\delta_T^2}, 1\right) \tag{15}$$

Combining equations (12) and (15) and taking into account the fact that $\delta_T \ll 1$ results in

$$w \sim \frac{1}{\delta_T^2} \tag{16}$$

The centrosymmetry of the cavity leads to $\Delta p_x/\delta_T \sim \Delta p_z$. Substituting this result, together with equation (13), into (14) yields

$$\left(w, \frac{u}{K}\right) \sim R_T \tag{17}$$

Combining equations (12), (16) and (17) results in

$$\left(\frac{1}{\delta_T^2}, \frac{1}{K\delta_T}\right) \sim R_T \tag{18}$$

From the above result it is found that when $K \gg \delta_T$ the thickness of the thermal boundary layer is given by $\delta_T \sim R_T^{-1/2}$ while when $K \ll \delta_T$ it is given by $\delta_T \sim (K R_T)^{-1}$. At this stage it is convenient to introduce a critical permeability ratio $K_{cr} \sim R_T^{-1/2}$ such that, depending on the value of the parameter K, the two following boundary layer regimes are possible:

$$\delta_T \sim R_T^{-1/2} \quad \text{when } K \gg K_{cr} \tag{19}$$

$$\delta_T \sim (K R_T)^{-1} \quad \text{when } K \ll K_{cr} \tag{20}$$

The first regime is a fully convective regime, which does not depend on the hydraulic anisotropy while the second one is a moderate convective regime for which the thickness of the thermal boundary layer δ_T depends on K.

The above results are valid under the classical conditions of the boundary layer regime, i.e. $\delta_T \ll 1$ and

$\delta_T \ll 1/A$ (distinct boundary layers). These conditions are satisfied if $R_T^{1/2} \gg 1$ and $R_T^{1/2} \gg A$, when $K \gg K_{cr}$, and if $K R_T \gg 1$ and $K R_T \gg A$ when $K \ll K_{cr}$.

The scaling properties of the mass transfer will be now discussed. Let δ_S be the dimensionless thickness of the solutal boundary layer. Upon integrating the equation of conservation of constituent (7) over δ_S it is found that

$$\frac{d}{dz}\int_0^\infty w(S - S_\infty)\,dx = \frac{1}{Le}\frac{\partial S}{\partial x}\bigg|_{x=0} \tag{21}$$

The above equation states that the vertical convective net transport of constituent is comparable to the horizontal diffusive transport of constituent. The order of magnitudes of this equilibrium yields

$$w\Delta S x \sim \frac{1}{Le}\frac{\Delta S}{\delta_S} \tag{22}$$

where ΔS is the concentration change across the solutal boundary layer.

In the above balance the order of magnitude of x can be estimated from the condition $x \sim \min(\delta_T, \delta_S)$. Depending on the value of the Lewis number the two following limiting situations can be considered:

(i) $Le \gg 1$ for which $\delta_S \ll \delta_T$: for this situation $x \sim \delta_S$ and it is readily found from equation (22) that $\delta_S \sim Le^{-1/2}\delta_T$. According to equations (19) and (20) it follows that

$$\delta_S \sim (Le R_T)^{-1/2} \quad \text{when } K \gg K_{cr} \tag{23}$$

$$\delta_S \sim (Le^{-1/2} R_T)^{-1} \quad \text{when } K \ll K_{cr} \tag{24}$$

(ii) $Le \ll 1$ for which $\delta_T \ll \delta_S$: for this situation $x \approx \delta_T$ and from equation (22) it follows that $\delta_S \approx Le^{-1}\delta_T$ such that

$$\delta_S \sim Le^{-1} R_T^{-1/2} \quad \text{when } K \gg K_{cr} \tag{25}$$

$$\delta_S \sim (K Le R_T)^{-1} \quad \text{when } K \ll K_{cr} \tag{26}$$

where, since $\delta_S \gg \delta_T$, the solutal boundary layer thickness must satisfy the conditions $\delta_S \ll 1$ and $\delta_S \ll 1/A$. Thus, it is required that $Le R_T^{1/2} \gg 1$ and $Le R_T^{1/2} \gg A$ when $K \gg K_{cr}$ and $K Le R_T \gg 1$ and $K Le R_T \gg A$ when $K \ll K_{cr}$.

3.2. Solute-driven flows

The class of flows dominated by the buoyancy forces which are mainly due to the gradients of concentration ($N \gg 1$) is now considered. Since the procedure to determine the scaling laws for this flow regime is similar to that discussed above only the final results are presented here.

From the governing equations (3), (4) and (7) it can be readily demonstrated that the dimensionless thickness of the solutal boundary layer δ_S is given by

$$\delta_S \sim R_S^{-1/2} \quad \text{when } K \gg K_{cr} \tag{27}$$

$$\delta_S \sim (K R_S)^{-1} \quad \text{when } K \ll K_{cr} \tag{28}$$

where $R_S = R_T N Le$ is the solutal Rayleigh number.

In order to determine the heat transfer scales the boundary layer must be integrated first. Here again the two possibilities $\delta_T \ll \delta_S$ and $\delta_T \gg \delta_S$ must be treated separately to yield

(i) $Le \ll 1$ for which $\delta_T \sim Le^{1/2}\delta_S$ (i.e. $\delta_T < \delta_S$) such that

$$\delta_T \sim Le^{1/2} R_S^{-1/2} \quad \text{when } K \gg K_{cr} \tag{29}$$

$$\delta_T \sim Le^{1/2} (K R_S)^{-1} \quad \text{when } K \ll K_{cr} \tag{30}$$

(ii) $Le \gg 1$ for which $\delta_T \sim Le\,\delta_S$ (i.e. $\delta_T < \delta_S$) such that

$$\delta_T \sim Le R_S^{-1/2} \quad \text{when } K \gg K_{cr} \tag{31}$$

$$\delta_T \sim Le (K R_S)^{-1} \quad \text{when } K \ll K_{cr} \tag{32}$$

It is noted that due to the symmetry of the governing equations (3)–(8) the above scales could have been deduced from those obtained for the heat-driven limit through the transformation $R_T \to R_S$, $N \to 1/N$, $\delta_T \to \delta_S$, $\delta_S \to \delta_T$ and $Le \to 1/Le$.

3.3. Heat and mass transfer scales

Results of practical interest are heat and mass transfer rates. From equations (10) and (11) it is clear that the order of magnitudes of the Nusselt and Sherwood numbers are given by $Nu \sim 1/\delta_T$ and $Sh \sim 1/\delta_S$, respectively. From the results obtained in the above sections the scaling properties of heat and mass transfer rates can be predicted for the two following regimes:

(i) Heat-driven flows ($N \ll 1$). For this situation, depending on the value of K, we have the following two possibilities:

- $K \ll K_{cr}$, for which

$$Nu \sim K R_T$$
$$Sh \sim K Le^{1/2} R_T \quad \text{when } Le \gg 1 \tag{33}$$
$$Sh \sim K Le R_T \quad \text{when } Le \ll 1$$

- $K \gg K_{cr}$, for which

$$\begin{aligned} Nu &\sim R_T^{1/2} \\ Sh &\sim (Le R_T)^{1/2} \quad \text{when } Le \gg 1 \\ Sh &\sim Le R_T^{1/2} \quad \text{when } Le \ll 1 \end{aligned} \tag{34}$$

The above results can be combined into the following equations:

$$\begin{aligned} Nu &\sim \frac{R_T^{1/2}}{\overline{K}} \\ Sh &\sim \frac{(Le R_T)^{1/2}}{\overline{K}} \quad \text{when } Le \gg 1 \\ Sh &\sim Le R_T^{1/2} \quad \text{when } Le \ll 1 \end{aligned} \tag{35}$$

where $\overline{K} = (1 + K_{cr}/K)$ and $K_{cr} \sim R_T^{-1/2}$.

(ii) Solute-driven flows ($N \gg 1$). Similarly, it is readily found that for this regime the Nusselt and Sherwood numbers are given by

$$\begin{aligned} Sh &\sim \frac{R_S^{1/2}}{\overline{K}} \\ Nu &\sim \frac{Le^{-1} R_S^{1/2}}{\overline{K}} \quad \text{when } Le \gg 1 \\ Nu &\sim \frac{Le^{-1/2} R_S^{1/2}}{\overline{K}} \quad \text{when } Le \ll 1 \end{aligned} \tag{36}$$

4. NUMERICAL SOLUTION

In this section we present a numerical solution of the complete governing equations (3)–(8). This solution, which can handle both boundary layer flows and flows without distinct boundary layers, will be used to confirm the validity of the results of the scale analysis presented in the preceding section.

The governing equations (3)–(8) are solved using the control volume finite-difference method described by Patankar [17]. The computation domain is divided into rectangular control volumes with one grid located at the centre of the control volume that forms a basic cell. The set of conservation equations are integrated over the control volumes, leading to a balance equation for the fluxes at the interface. A hybrid scheme is used to discretise the equations, false transient procedure is used in order to obtain permanent solution. The system of equations formulated in terms of primitive variables is solved using the tridiagonal matrix algorithm (TDMA). The pressure–velocity coupling in the momentum equation needs iterative procedure based on a pressure correction method where SIMPLER algorithm is coupled to the SIMPLEC algorithm (Van Doormaal and Raithby [18]), for faster convergence.

Non-uniform grids are used in the program, allowing a fine grid spacing near the two vertical walls. Convergence with mesh size was verified by employing coarser and finer grids on selected test problems. The computations reported in this paper have been performed using more than a 61×61 grid. The convergence criterion is based on both maximum error of continuity equation and the average quadratic residual over the whole domain for each equation. It is assumed that convergence is reached when the maximum error is less than 10^{-6}.

The validation of the numerical code was performed over a large range of parameters. Typical results are presented in *tables I* and *II* for the case of isotropic and

TABLE I
Present Nusselt and Sherwood numbers compared with those of Trevisan and Bejan [19] and Goyeau et al. [20] for the case of isotropic porous media.

R_T		100	200	400	1 000	2 000	Le
Present work	Nu	3.11	4.96	7.77	13.48	19.89	10
	Sh	13.24	19.83	29.36	48.20	69.08	
Trevisan and Bejan [19]	Nu	3.27	5.61	9.69	–	–	
	Sh	15.61	23.23	30.73	–	–	
Goyeau et al. [20]	Nu	3.11	4.96	7.77	13.47	19.90	
	Sh	13.25	19.86	28.41	48.32	69.29	
Present work	Nu	–	–	–	13.48	19.89	100
	Sh				139.93	195.37	
Goyeau et al. [20]	Nu	–	–	–	13.47	19.90	
	Sh				140.65	196.62	

TABLE II
Present Nusselt numbers compared with those represented by Ni and Beckerman [5] for the case of anisotropic porous media.

$K = K_x/K_z$	10^{-3}	10^{-2}	10^{-1}	1	10	10^2	10^3
Present work	119.32	80.62	37.56	13.48	4.17	1.29	1.00
Ni and Beckermann [5]	118.72	80.34	37.37	13.41	4.17	1.30	1.01

anisotropic porous media, respectively. In general, the results are in good agreement with those of Ni and Beckermann [5] and Goyeau et al. [20], thereby providing validation to our simulations. However, it seems that the results proposed by Trevisan and Bejan [19] overestimate the Nusselt and Sherwood numbers at high porous number ($R_T = 400$).

5. RESULTS AND DISCUSSION

As was already noted above, the system considered here is governed by five nondimensional groups, namely, the thermal Rayleigh number R_T, buoyancy ratio N, Lewis number Le, anisotropy ratio K and aspect ratio A. Due to the abundance of parameters all the numerical results presented here were obtained only for the case of a square cavity ($A = 1$).

Figure 2(a) illustrates the effect of the permeability ratio on the vertical velocity profile at mid-height of the cavity for $R_T = 10^4$, $N = 0$ and $Le = 10$. For a given value of K the numerical results indicate that the velocity at the wall is maximum, in agreement with Darcy's model which allows the fluid to slip on a solid boundary, and then drops back to zero in the core region of the enclosure. Upon increasing K from 10^{-2} to 10^2, it is seen from *figure 2(a)* that the value of the maximum velocity ($x = 0$) increases from 700 to 6 200, indicating that the convective circulation within the cavity is promoted. This behaviour can be explained by the fact that for a fixed value or R_T (i.e. K_z) an increase in K can be interpreted as an increase in the permeability K_x, resulting in a stronger convective flow. Naturally, the reverse is true when the value of K is made very small. For this reason it is observed from *figure 2(b)* that both the Nusselt and Sherwood numbers approach the pure diffusive regime ($Nu \to 1$ and $Sh \to 1$) when K is made small enough. This limit is reached approximately when $K \approx 5{\cdot}10^{-4}$ for Nu and $K \approx 5{\cdot}10^{-5}$ for Sh. As expected, Nu and Sh increase with increasing K since, as explained above, the buoyancy-induced flow becomes stronger with K. However, it is seen from *figure 2(b)* that both Nu and Sh reach maximum values when $K \geq 1$ and

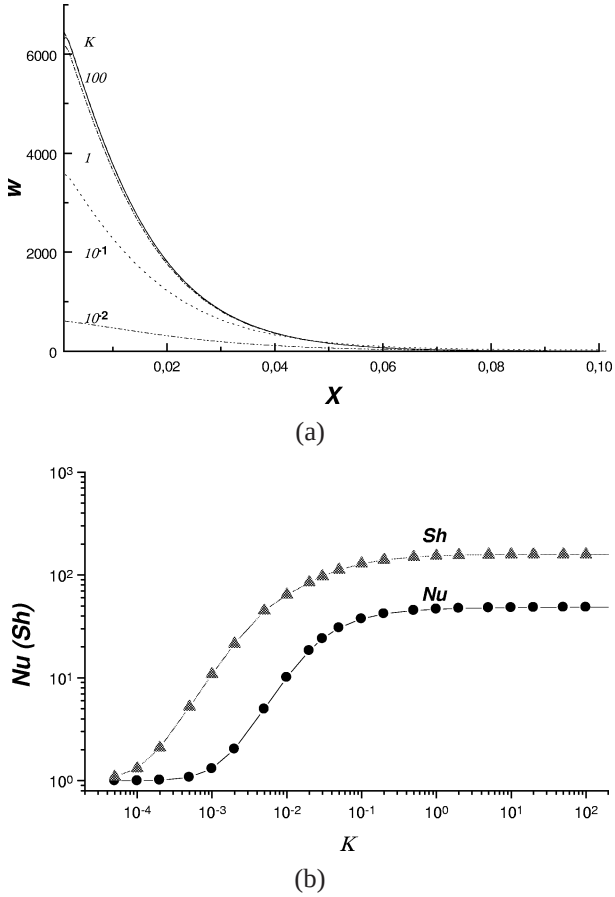

Figure 2. Effect of permeability ratio K, for $A = 1$, $R_T = 10^4$, $N = 0$ and $Le = 10$, on (a) vertical velocity profile at mid-height of the cavity and (b) Nusselt and Sherwood numbers.

are independent of this parameter when this latter is made larger. This situation corresponds to a porous medium with an isotropic permeability K_z.

The above results show the existence of three regimes for the evolution of the heat and mass transfer with the permeability ratio. Thus, we have a diffusive regime for low values of K, an intermediate regime for intermediate values of K in which both Nu and Sh increase with increasing K and a convective regime for high values

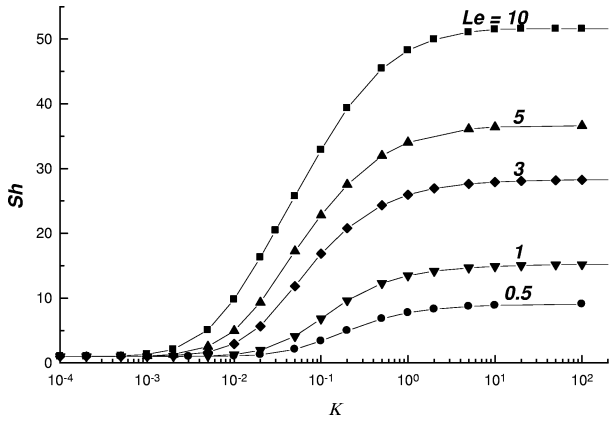

Figure 3. Effects of permeability ratio K and Lewis number Le on Sherwood number for $A = 1$, $R_T = 10^3$ and $N = 0$.

of K where Nu and Sh reach a maximum and are found to be independent of the permeability ratio.

Figure 3 displays the Sherwood number as a function of K for various values of Le at $R_T = 10^3$ and in the case of thermal driven flow ($N = 0$). For a given value of Le the evolution of Sh with K, i.e. the existence of three different regimes, is similar to what has been discussed in *figure 2*. On the other hand, for a given value of K, it is seen that the mass transfer increases with the Lewis number. This follows from the fact that an increase in Le corresponds to a decrease in the mass diffusivity, i.e. to a reduction in the solutal boundary layer thickness leading to a higher Sherwood number. It is also observed from *figure 3* that, as Le is increased, a smaller value of K is required to reach the diffusive regime. Thus, this latter is reached for $K \approx 10^{-2}$ when $Le = 1$ and for $K \approx 10^{-3}$ when $Le = 10$.

The effects of K on both Nu and Sh will be now discussed for the case of $N = 0$ for which the buoyancy forces that drive the fluid motion are mainly due to the gradients of temperature. In this limit, on the basis of the scale analysis discussed before, the numerical results obtained in this study for $Le = 10$ were correlated in order to predict the influence of R_T, Le and K on the Nusselt and Sherwood numbers. In the range of the governing parameters investigated here the following correlations were obtained:

$$Nu = 1 + 0.27\overline{K}^{-1} R_T^{0.57} \tag{37}$$

where $\overline{K} = (1 + K_{cr}/K)$ and $K_{cr} = 4.5 R_T^{-0.52}$, and

$$Sh = 1 + 0.47\overline{K}^{-1} (R_T Le)^{0.51} \tag{38}$$

where $K_{cr} = 4 R_T^{-0.62}$.

In the case of purely thermal natural convection it was demonstrated by Simpkins and Blythe [21] that, in the boundary layer regime, the heat transfer is given by

$$Nu = 0.51 R_T^{0.51} \tag{39}$$

Equation (37) for $\overline{K} = 1$ (isotropic porous media) predicts a lower mass transfer that equation (39).

In the case of double-diffusive convection in a square cavity it was found by Goyeau et al. [20] that the mass transfer due to purely thermal natural convection can be predicted by the following correlation:

$$Sh = 0.40 (R_T Le)^{0.51} \tag{40}$$

A good agreement is found between equations (38) and (40) when $\overline{K} = 1$, i.e. for isotropic porous media.

The effects of varying the thermal Rayleigh number and permeability ratio on the heat and mass transfer, Nu and Sh, are illustrated in *figure 4* for $N = 0$ and $Le = 10$. The solid symbols in these graphs are the results of the numerical simulation and are seen to be in good agreement with the correlations (37) and (38). These correlations are observed to predict accurately the three different regimes discussed before despite the large range of parameters cover in *figure 4*.

In the limit $N \to \infty$, for which the buoyancy forces that drive the flow are mainly due to gradients of solute, the numerical results obtained in this study were also correlated to yield

$$Sh = 1 + 1.26\overline{K}^{-1} R_S^{0.42} \tag{41}$$

where $K_{cr} = R_S^{-0.42}$.

For an isotropic porous medium ($\overline{K} = 1$) the following correlation, valid in the boundary layer regime, was proposed by Goyeau et al. [20]:

$$Sh = 0.75 R_S^{0.46} \tag{42}$$

Figure 5 shows a comparison between equations (41) and (36) and the numerical results obtained for $R_T = 10^3$, $Le = 10$ and $N = 0$, 10, 20 and 30. For completeness the results obtained in *figure 3(b)* for $N = 0$ are also presented in this graph. Here again it is observed that the correlation proposed in this study to predict the mass transfer in the solute-driven flow limit is in good agreement with the numerical results.

All the above results were obtained by modelling the momentum equation in the porous medium using Darcy's law. For isotropic porous media it has been

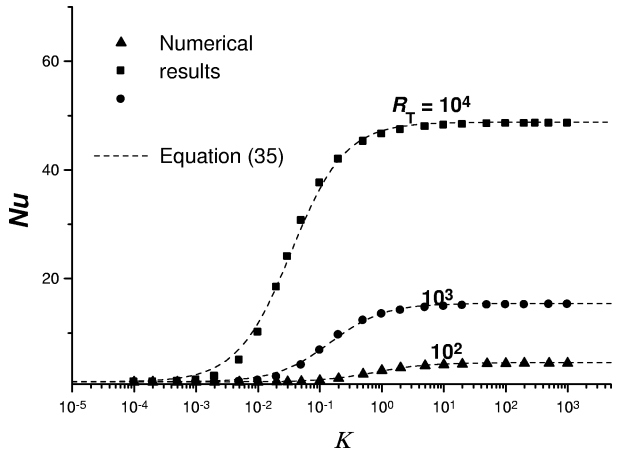

(a)

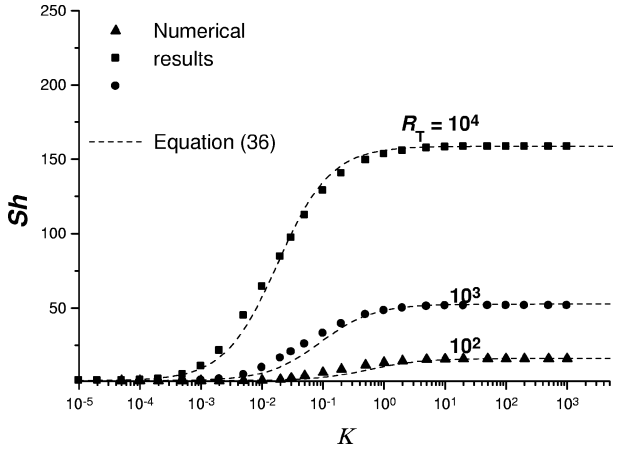

(b)

Figure 4. Effects of permeability ratio K and Rayleigh number R_T, for $N = 0$, $Le = 10$, on (a) Nusselt number and (b) Sherwood number.

demonstrated in the past by many authors (see, for instance, Tong and Subramanian [22] and Vasseur and Robillard [23]), that Darcy's law is, indeed, a good approximation for low-porosity media; i.e. when the Darcy number *Da* based on the height of the porous medium is less than approximately 10^{-3}. However, for higher values of *Da*, Darcy's model may overpredict the flow rate, because it cannot account for the no-slip boundary condition on rigid boundaries. To consider the boundary effect, which may become important in porous media with high porosities, Brinkman's extension of Darcy's law should be used. Recently the Brinkman-extended Darcy model has been considered by Degan and Vasseur [12] to study natural convection heat transfer in a vertical anisotropic porous layer and by Goyeau et

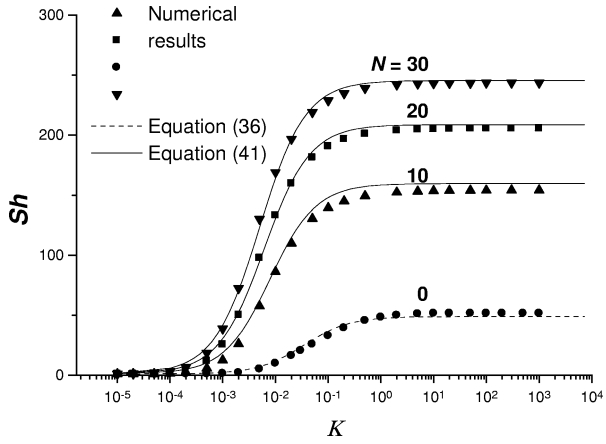

Figure 5. Effects of permeability ratio K and buoyancy ratio N, for $R_T = 10^3$ and $Le = 10$, on Sherwood number.

al. [20] to study double-diffusive convection in confined isotropic porous media. However, no results are available concerning the influence of the Darcy number on double-diffusive convection in a cavity filled with an anisotropic porous medium.

In terms of the nondimensional variables, equation (2), the Darcy–Brinkman formulation of the momentum equation can be written as follows (see, for instance, [23]):

$$u = -K\left[\frac{\partial p}{\partial z} + Da\,\lambda\nabla^2 u\right] \tag{43}$$

$$w = -\frac{\partial p}{\partial x} + R_T(T + NS) + Da\,\lambda\nabla^2 w \tag{44}$$

where $Da = K_z/H^2$ is the Darcy number based on permeability K_z and $\lambda = \mu_{\text{eff}}/\mu$ is the relative viscosity. In the present study the value of the apparent dynamic viscosity μ_{eff} is taken, as a first approximation, equal to μ (i.e. $\lambda = 1$).

The fluid, in the Darcy–Brinkman formulation, is required to satisfy the no-slip boundary condition on rigid boundaries. Thus, the nondimensional boundary conditions over the walls of the enclosure are now given by

$$\begin{aligned}
&x = 0, && u = w = 0, && T = 0.5, && S = 0.5\\
&x = \frac{1}{A}, && u = w = 0, && T = -0.5, && S = -0.5\\
&z = 0 \text{ or } 1, && u = w = 0, && \frac{\partial T}{\partial z} = 0, && \frac{\partial S}{\partial z} = 0
\end{aligned} \tag{45}$$

The solution of the governing equations (3), (6), (7), (43) and (44), under boundary conditions (45), was obtained using the numerical procedure described before.

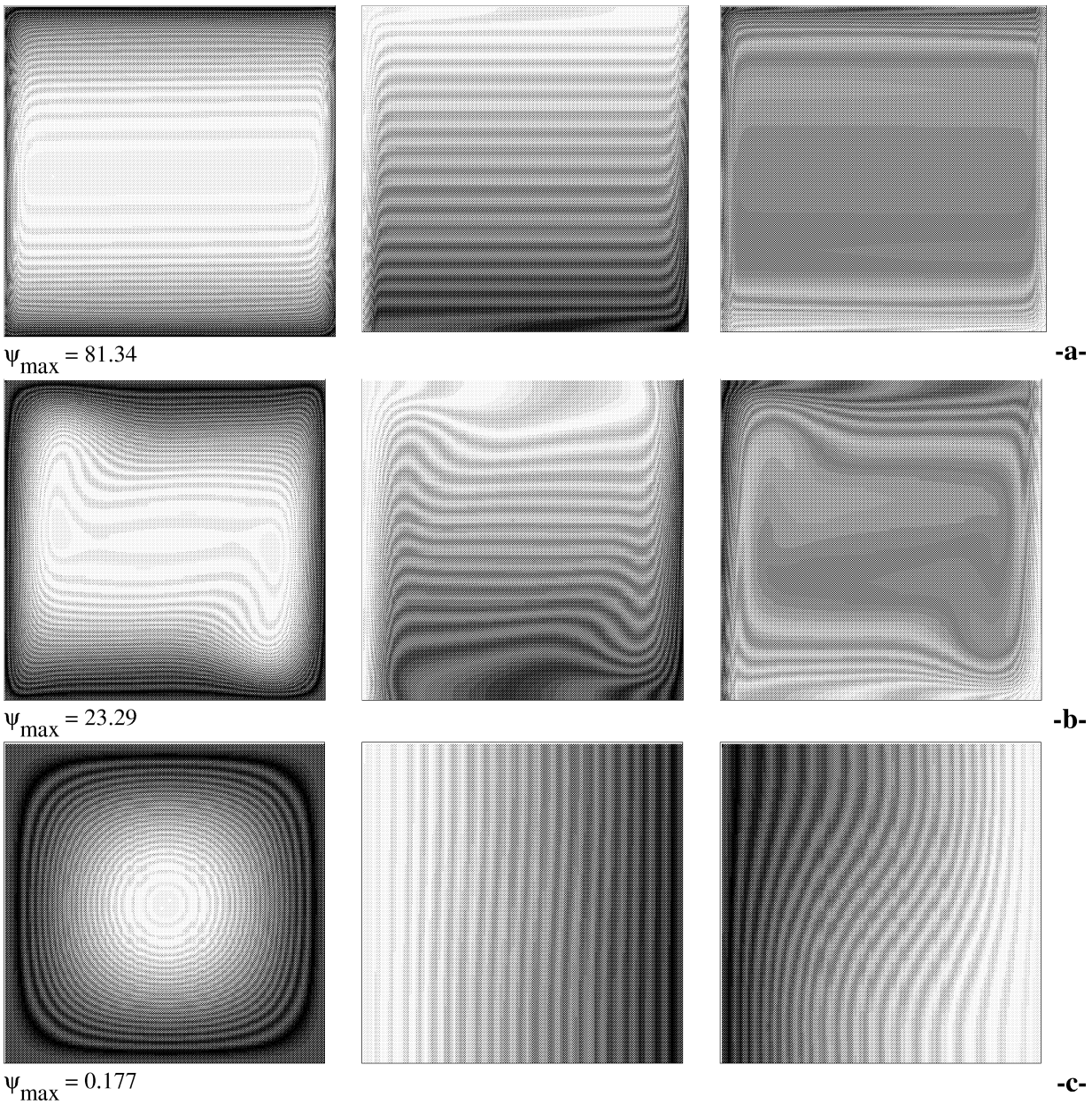

Figure 6. Streamlines (left), isotherms (centre) and constant-concentration lines (right), for $R_T = 10^4$, $N = 0$, $Le = 10$ and $K = 10^3$, for (a) $Da = 10^{-7}$, (b) $Da = 10^{-2}$ and (c) $Da = 10^2$.

Figure 6 illustrates typical numerical results for the flow (left), temperature (centre) and concentration (right) fields for $R_T = 10^4$, $K = 10^3$, $Le = 10$, $N = 0$ and various values of Da. For each map of *figure 6*, the increments between adjacent streamlines, isotherms and isoconcentrates are $\Delta\phi = (\phi_{max} - \phi_{min})/20$, where ϕ stands for ψ, T and S, respectively. *Figure 6(a)* shows the results obtained for $Da = 10^{-5}$. A clockwise rotating cell fills up the entire cavity with hydrodynamic boundary layers along the vertical walls and a motionless core region. The temperature field indicates the existence of thermal boundary layers along the vertical isothermal walls, the temperature variation being large in these boundary regions. It is also noticed that the temperature

in the core of the cavity is nearly constant in the horizontal direction and varies almost linearly in the vertical direction. The isoconcentrate field, on the other hand, indicates that the concentration boundary layer is sharper than the thermal boundary layer. Also, the concentration field in the core of the cavity is noted to be almost uniform. This is due to the relatively high Lewis number considered here for which the mass diffusivity is considerably lower than the thermal diffusivity ($Le = 10$). These results are qualitatively similar to those reported in the literature on the basis of Darcy's law, for low-porosity media, i.e. when *Da* is small enough such that the viscous terms, which are responsible for the boundary effects, are negligibly small. As the Darcy number is increased, the boundary frictional resistance becomes progressively significant and adds to the bulk frictional drag induced by the solid matrix to slow the convection motion. Indeed, it is seen from *figure 6* that the strength of the overall convective flow becomes weaker and weaker as the value of *Da* is made larger. For instance, the maximum stream function drops from $\psi_{\max} = 81.34$ to $\psi_{\max} = 0.18$ as the value of the Darcy number is increased from $Da = 10^{-5}$ to $Da = 10^{2}$. It is noted that the flow pattern illustrated in *figure 6(c)*, for which $Da = 10^{2}$, corresponds approximately to that of a pure fluid. For this situation the relevant thermal Rayleigh number $Ra_{\mathrm{T}} = g\beta_{\mathrm{T}}\Delta T' H^3/(\alpha\nu)$ is given by $Ra_{\mathrm{T}} = R_{\mathrm{T}}/Da = 10$ which is relatively small. For this reason, convection is very weak and the heat and mass transfer across the cavity are almost purely diffusive as indicated by the nearly vertical isotherms and isoconcentrates of *figure 6(c)*.

Figure 7 shows the effect of varying the Darcy number *Da* and permeability ratio K on both *Nu* and *Sh* for $R_{\mathrm{T}} = 10^4$, $N = 0$ and $Le = 10$. The results predicted by Darcy's law, equations (35)–(36), are indicated as dotted lines for comparison. As expected, when the Darcy number is small enough ($Da \leq 10^{-7}$) the numerical results obtained with the Brinkman model are in agreement with Darcy's law. Upon increasing the permeability of the porous medium (i.e. *Da*) it is seen from *figure 7* that both the Nusselt and Sherwood numbers drop considerably and become less and less affected by K. This behaviour results from the fact that, as the permeability of the porous medium *Da* is increased, the boundary frictional resistance becomes gradually more important and adds to the bulk frictional drag induced by the solid matrix to slow down the flow circulation within the cavity. When *Da* is high enough, i.e. when the resistance resulting from the boundary effects is predominant with respect to that due to the porous matrix, the present solution approaches that for a pure viscous fluid, in the absence of inertia effects, and the anisotropy of the porous medium becomes

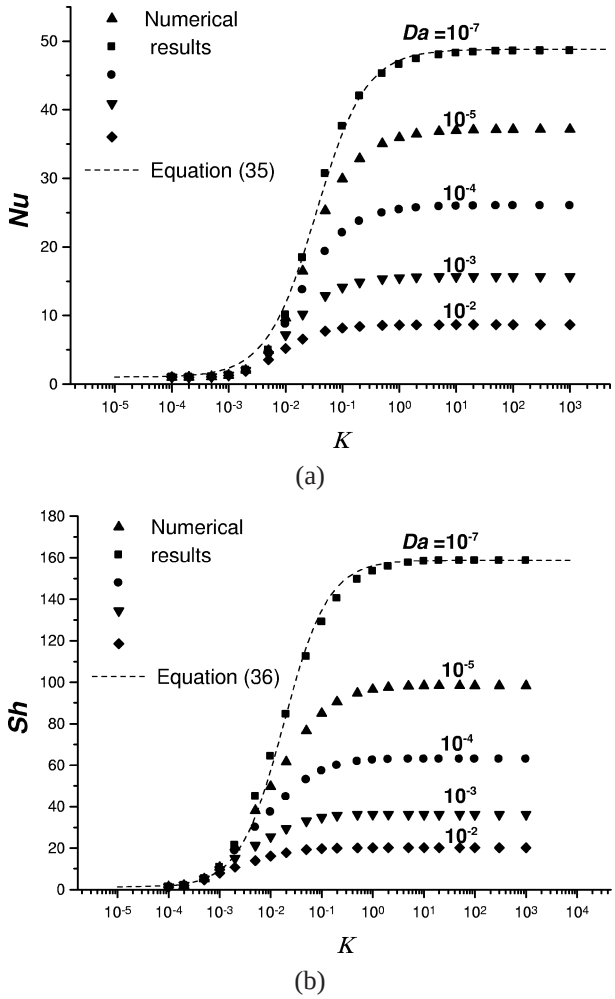

Figure 7. Effects of permeability ratio K and Darcy number *Da*, for $R_{\mathrm{T}} = 10^4$, $N = 0$ and $Le = 10$ on (a) Nusselt number and (b) Sherwood number.

almost negligible. Similar results have been reported by Degan and Vasseur [12] while considering thermal convection in a vertical anisotropic porous layer on the basis of the Brinkman-extended Darcy model.

6. CONCLUSIONS

A study has been made of double-diffusive natural convection in a square porous cavity with horizontally cooperating imposed temperature and concentration gradients. The porous medium is assumed to be hydrodynamically anisotropic with the principal axes of anisotropic permeability aligned with the gravity vector. Scale analysis is applied to the two extreme cases of heat-driven and

solute-driven natural convection. Correlations for the average Nusselt and Sherwood numbers, based on numerical results obtained by solving the complete governing equations, are proposed. These numerical results indicate the existence of three regimes, namely, a diffusive one for low values of K, a transition regime when Nu and Sh increase as the value of K is made larger and an asymptotic regime where Nu and Sh become independent of K and reach constant values as the value of K is made large enough. The transition between the different regimes depends on the thermal Rayleigh number R_T, buoyancy ratio N and the Lewis number Le. The correlations proposed in this study are found to be in good agreement with the numerical results and this for a large range of the governing parameters.

The boundary effects, which are expected to be important in porous media with high porosities, have also been investigated in this study on the basis of the Brinkman-extended Darcy model. The numerical results indicate that when Da is small enough the above results, obtained on the basis of Darcy's law, are valid. For intermediate values of Da the boundary frictional resistance becomes gradually important and slows down the convective motion. As a result, the effects of the anisotropic permeability of the porous medium on the convection heat transfer become less and less important.

REFERENCES

[1] Nilsen T., Storesletten L., An analytical study on natural convection in isotropic and anisotropic porous channels, J. Heat Tran. 112 (1990) 396–401.

[2] Nield D.A., Bejan A., Convection in Porous Media, 2nd ed., Springer Verlag, New York, 1999.

[3] Ingham D.B., Pop I., Transport Phenomena in Porous Media, Pergamon, 1998.

[4] Kimura S., Masuda Y., Kazuo Hayaski T., Natural convection in an anisotropic porous medium heated from the side (Effects of anisotropic properties of porous matrix), Heat Transfer Japan 22 (1993) 139–153.

[5] Ni J., Beckermann C., Natural convection in a vertical enclosure filled with anisotropic porous media, J. Heat Tran. 113 (1991) 1033–1037.

[6] Tyvand P.A., Storesletten L., Onset of convection in an anisotropic porous medium with oblique principal axes, J. Fluid Mech. 226 (1991) 371–382.

[7] Zhang X., Nguyen T.H., Kahawita R., Convection flow and heat transfer in an anisotropic porous layer with principal axes non-coincident with the gravity vector, in: Proc. ASME Winter Annual Meeting, Fundamentals of Natural Convection, HTD, Vol. 264, 1993, pp. 79–86.

[8] Mamou M., Mahidjiba A., Vasseur P., Robillard L., Onset of convection in an anisotropic porous medium heated from below by a constant heat flux, Int. Comm. Heat Mass Tran. 25 (1998) 799–808.

[9] Zhang X., Convective heat transfer in a vertical porous layer with anisotropic permeability, in: Proc. 14th Canadian Congress of Applied Mechanics, Vol. 2, 1993, pp. 579–580.

[10] Degan G., Vasseur P., Bilgen E., Convective heat transfer in a vertical anisotropic porous layer, Int. J. Heat Mass Tran. 38 (1995) 1975–1987.

[11] Degan G., Vasseur P., Natural convection in a vertical slot filled with an anisotropic porous medium with oblique principal axes, Numerical Heat Transfer A 30 (1996) 397–412.

[12] Degan G., Vasseur P., Boundary layer regime in a vertical porous layer with anisotropic permeability and boundary effects, Int. J. Heat Fluid Flow 18 (1997) 334–343.

[13] Tyvand P.A., Thermohaline instability in anisotropic porous media, Water Resources Res. 16 (1980) 325–330.

[14] Nguyen H.D., Paik S., Douglass R.W., Study of double-diffusive convection in layered anisotropic porous media, Numerical Heat Transfer B 26 (1994) 489–505.

[15] Bera P., Eswaran V., Singh P., Numerical study of heat and mass transfer in an anisotropic porous enclosure due to constant heating and cooling, Numerical Heat Transfer A 34 (1998) 887–905.

[16] Bejan A., Khair K.R., Heat and mass transfer by natural convection in a porous medium, Int. J. Heat Mass Tran. 28 (1985) 909–918.

[17] Patankar S., Numerical Heat Transfer and Fluid Flow, Hemisphere, New York, 1980.

[18] Van Doormaal J.P., Raithby G.D., Enhancement of the simple method for predicting incompressible fluid flows, Numerical Heat Transfer 7 (1984) 147–163.

[19] Trevisan O.V., Bejan A., Natural convection with combined heat mass transfer buoyancy effects in a porous medium, Int. J. Heat Mass Tran. 28 (1985) 1597–1611.

[20] Goyeau B., Songbe J.P., Gobin D., Numerical study of double diffusive natural convection in a porous cavity using the Darcy–Brinkman formulation, Int. J. Heat Mass Tran. 39 (1996) 1363–1378.

[21] Simpkins G., Blythe P.A., Convection in porous layer, Int. J. Heat Mass Tran. 23 (1980) 881–887.

[22] Tong T.W., Subramanian E., A boundary layer analysis for natural convection in a vertical porous enclosure — use of the Brinkman–extended Darcy model, Int. J. Heat Mass Tran. 30 (1985) 563–571.

[23] Vasseur P., Robillard L., The Brinkman model for boundary-layer regime in a rectangular cavity with uniform heat flux from the side, Int. J. Heat Mass Tran. 30 (1987) 717–727.